ERS-1 SAR backscatter from nilas and young ice during freeze-up

by Lars M.H. Ulander, Anders Carlström and Jan Askne

Department of Radio and Space Science
Chalmers University of Technology
S-412 96 Göteborg, Sweden

ABSTRACT

Nilas and young ice have highly variable backscatter signatures in ERS-1 SAR images. We have investigated their evolution during a 2-week period in September 1991 when the air temperature dropped from 0° to -16°C. Field observations show that very different surface conditions develop due to the temperature and precipitation history, i.e. frost flowers, saline snow and slush. The highest backscatter was found for rough and wet saline snow, probably formed by snow falling on frost flowers, whereas the lowest backscatter was found for slush-covered ice. Newly formed frost flowers were found to have a backscattering coefficient close to that of slush. Comparison with theoretical backscattering models show reasonable agreement for most cases.

1. INTRODUCTION

Freezing of open leads is an important effect for the energy exchange between ocean and atmosphere. The heat flux is one or two orders of magnitude larger for thin ice (0-0.4m) compared to thick ice (3-4m) (Maykut 1978). Ice with thickness between 0.1-0.8m provides about 75% of the total annual heat loss in the Arctic (Maykut 1982) although their average cover is only about 10% (Thorndike *et al.* 1975).

Satellite synthetic-aperture radar (SAR) is a promising technique for measuring many sea ice parameters of importance for climate monitoring. However, there is still a lack of knowledge concerning the relation between radar backscattering and the physical properties of the ice. Detailed *in situ* measurements of the ice is thus a necessity as part of microwave remote sensing experiments. Several recent papers have investigated theoretical sea ice scattering models by comparing simultaneous radar measurements with theoretical models (Kim *et al.* 1985, Livingstone and Drinkwater 1991, Ulander *et al.* 1992, Winebrenner *et al.* 1992, Carlström and Ulander 1993). This paper approaches the problem of measuring and modelling thinner ice forms, i.e. nilas and young ice, which often are covered by frost flowers, saline snow and slush.

The International Arctic Ocean Expedition 1991 (ARCTIC-91) was an expedition with three surface vessels to the high Arctic between 1 August and 14 October 1991 (see Fig. 1). The Remote Sensing and Sea Ice programme on the Swedish icebreaker *Oden* had the objective of developing remote sensing techniques for ice parameter retrieval using the ERS-1 C-band SAR. The approach was to make *in situ* measurements of both physical and microwave properties. The ice and snow properties were sampled with emphasis on parameters relevant for radar scattering, i.e. surface roughness, snow depth, wetness, and density, as well as brine and air void content of the ice. The coverage of the ERS-1 SAR in the northern hemisphere is limited to south of N 84,6° and the measurement program was therefore concentrated to this area. A lot of measurements were also made north of N 84,6° in order to obtain statistics of the large-scale variations of sea ice properties (Carlström and Ulander 1993). A total of twenty-two field stations were completed, of which seven were within the ERS-1 SAR swath.

The paper first describes the basic methodology, i.e. radiometric calibration of the ERS-1 SAR images in Section 2 and the backscattering models in Section 3. Sections 4 and 5 summarises the experimental conditions and the observed signature variations, respectively. Measurements and models of the backscattering coefficient are then compared in Section 6, followed by a short discussion of the results in Section 7 and concluding remarks in Section 8.

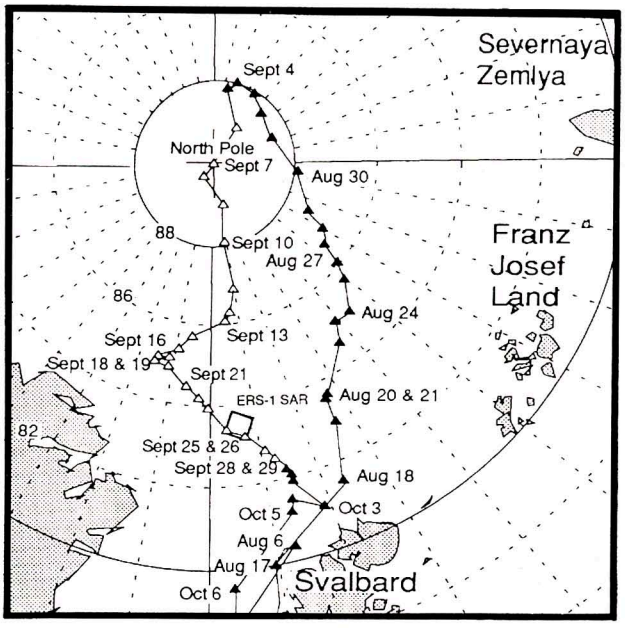

Fig. 1 - Map showing the expedition cruise track, and the location of field stations and ERS-1 SAR images

2. RADIOMETRIC CALIBRATION

Absolute radiometric calibration of the ERS-1 SAR images was ensured by deployment of two precision radar reflectors. Each reflector had a side length of 1.72 m and was mounted on a platform that was adjustable in both azimuth and elevation. The theoretical radar cross section of the trihedrals was 40.6 dBm^2 at 5.3 GHz. The precision of the calibration is mainly determined by the single-look signal-to-clutter ratio, which gives ±0.3 dB by assuming a worst case background with σ° = -10 dB. The accuracy of the calibration is more difficult to estimate since it depends critically on the geometrical accuracy and rigidness of the reflectors. Although the radar cross sections of the two reflectors have not been verified by measurements, the accuracy of the radar cross section is believed to be ±0.5 dB.

The two radar reflectors were deployed on five of the ERS-1 field stations. The azimuth and elevation angles were generally within a few degrees from the line-of-sight to the SAR implying that the misalignment can be neglected. Unfortunately, helicopter transportation caused a deformation of the bottom plate by about 1 cm which will affect the radar cross section. The reflectors were adjusted accordingly after the deformation was discovered. It is believed that the reflector measurements on 20 August and 29 September are still satisfactory.

The backscattering coefficient σ° can be determined according to (Laur 1992, Ulander 1992)

$$\langle\sigma^\circ\rangle = \frac{f}{K}\left(\langle DN^2\rangle - \langle DN_n^2\rangle\right) \qquad (1)$$

where < > denotes spatial averaging, K is the calibration constant determined from the radar reflector responses (Ulander 1991), f is a range-dependent correction, and DN and DN_n are the pixel values of the distributed scatterer and noise, respectively. The definition of the range correction f is different for different ESA products. In the present paper, we have used precision (PRI) SAR images processed at UK-PAF prior to 1 September 1992, for which the following definition applies

$$f = \frac{G^2(\vartheta_r)\sin\theta}{G^2(\vartheta)\sin\theta_r} \qquad (2)$$

where θ is the local incidence angle ($\theta_r = 23^\circ$) and G is the antenna gain pattern as a function of elevation angle from nadir ϑ ($\vartheta_r = 20.35^\circ$ is the antenna boresight angle). We have determined the calibration constant K to 58.6 ± 0.3 dB using the radar reflectors on 20 August and 29 September which is 0.9 dB lower than the ESA calibration constant. The difference could indicate a systematic effect associated with high latitudes and large thermal gradients along the satellite orbit, but no investigation of these effects have been made to our knowledge. The number of data points in our analysis is, however, only four and we have therefore chosen to adopt the official ESA calibration constant, i.e. K = 59.5 dB (Laur 1992). The calibration accuracy is expected to be at least ± 1 dB.

3. BACKSCATTERING MODEL

The backscattering coefficient of snow-covered sea ice may be expressed as (Kim *et al.* 1984)

$$\sigma^0(\theta) = \sigma^0_{ss}(\theta) + T^2_{as}(\theta)\left\{\sigma^0_{sv}(\theta') + \frac{1}{L^2_s(\theta')}\left[\sigma^0_{is}(\theta') + T^2_{si}(\theta')\,\sigma^0_{iv}(\theta'')\right]\right\} \qquad (3)$$

where the contributing backscattering coefficients are denoted with σ^0_{ss} for the snow surface, σ^0_{sv} for the snow volume, σ^0_{is} for the ice surface, and σ^0_{iv} for the ice volume. The power transmission coefficients for the air/snow and snow/ice interfaces are denoted T_{as} and T_{si}, respectively,

and L_s is the loss factor of the snow layer. The incidence angle is θ, and the refracted angles in the snow and ice volumes are θ', and θ'', respectively. Note that the formulation according to (3) neglects interactions between surface and volume scattering, which are usually small for like polarisation.

In our case, the snow cover was wet and saline in those cases where snow was encountered. Hence, the loss factor of the snow layer was large, which make us conclude that both volume scattering from the snow and ice scattering are negligible. A few of the ice sheets were bare and thus it is scattering from the ice surface that is dominant since the penetration depth is very small in saline ice. We may therefore simplify the model to account for surface scattering only, and where the scattering surface is either saline snow, slush or ice. The magnitude of the scattering is controlled by the roughness of the surface and by the dielectric constant of the surface.

With the assumption that the surface height is described by a Gaussian stationary random process, we apply the integral-equation model (IEM) for computing the surface backscattering coefficient (Fung *et al.* 1992)

$$\sigma_s^0(\theta) = \frac{k^2}{2} \exp(-2s^2 k_z^2) \sum_{n=1}^{\infty} s^{2n} \left| I_{pp}^n \right|^2 \frac{W^n(-2k_x, 0)}{n!} \quad (4)$$

where s is the rms height, $k_z = k\cos\theta$ and $k_x = k\sin\theta$. The coefficients I^n_{pp} are functions of dielectric constant, incidence angle, and radar wave number k. W^n is the Fourier transform of the nth power of the two-dimensional surface autocorrelation function. The model is valid for $s/l < 0.4$, where l is the correlation length.

The dielectric properties of the ice depend on the volumetric fractions of liquid brine and air, which are computed from temperature, salinity, and density measurements using the method described in (Cox and Weeks 1983). We have assumed that this method may be applied to calculate the liquid brine and air content of saline snow, frost flowers and slush as well.

The complex dielectric constant of sea ice is calculated using the empirical equations given in (Vant *et al.* 1978)

$$\varepsilon' = 3.05 + 7.2\,\upsilon$$
$$\varepsilon'' = 0.024 + 3.29\,\upsilon \quad (5)$$

where υ is the volumetric fraction of liquid brine. These equations for first year ice were determined for a frequency of 4.0 GHz but are also applicable at 5.3 GHz since the frequency dependence is relatively weak for C-band frequencies.

The dielectric properties of snow have been reviewed in (Hallikainen *et al.* 1986). They propose a Polder-van Santen model in which dry snow is mixed with water inclusions and show it to be accurate for water volume fractions up to 12%. The shape of the water inclusions are varying with increasing wetness and approach disc-like forms for high water contents. To be able to use this model for saline snow, we replace the dielectric constant of pure water with that of brine (Stogryn and Desargant 1985).

Frost-flowers have a very different shape from snow and the dielectric properties are probably different. For newly formed frost flowers, we use the same mixing model as for saline snow which we believe estimates the dielectric constant to a reasonable value. For old frost flowers, which had developed into a solid rough ice surface, we instead use the dielectric model for sea ice according to (5).

When the brine content of saline snow becomes too high, the snow collapses to form a slush layer which may be assumed to have a liquid fraction above 30-40 %. Salinities as high as 150 ‰ have been measured in the Arctic (Drinkwater and Crocker 1988), which results in a brine volume fraction of 100 % at a temperature of -10°C. The dielectric constant of slush has to our knowledge never been investigated experimentally. We propose a Polder-van Santen model in which brine is a host medium for spherical ice inclusions. We do not include air in this model, since the air content in slush is small and would have a minor effect on the dielectric constant.

4. GENERAL CONDITIONS DURING THE EXPERIMENT

From the beginning of September there was a decreasing trend in the air temperature as shown in Fig. 2. This resulted in new ice growth which accelerated as the temperature dropped. Air temperatures around 0°C occurred on 22-23 September which resulted in melting and brine drainage. Falling snow occurred relatively seldom which resulted in a thin snow cover. Snow fall was recorded on an hourly basis and is also shown in Fig. 2. The major part of the snow fell between 27 and 30 September.

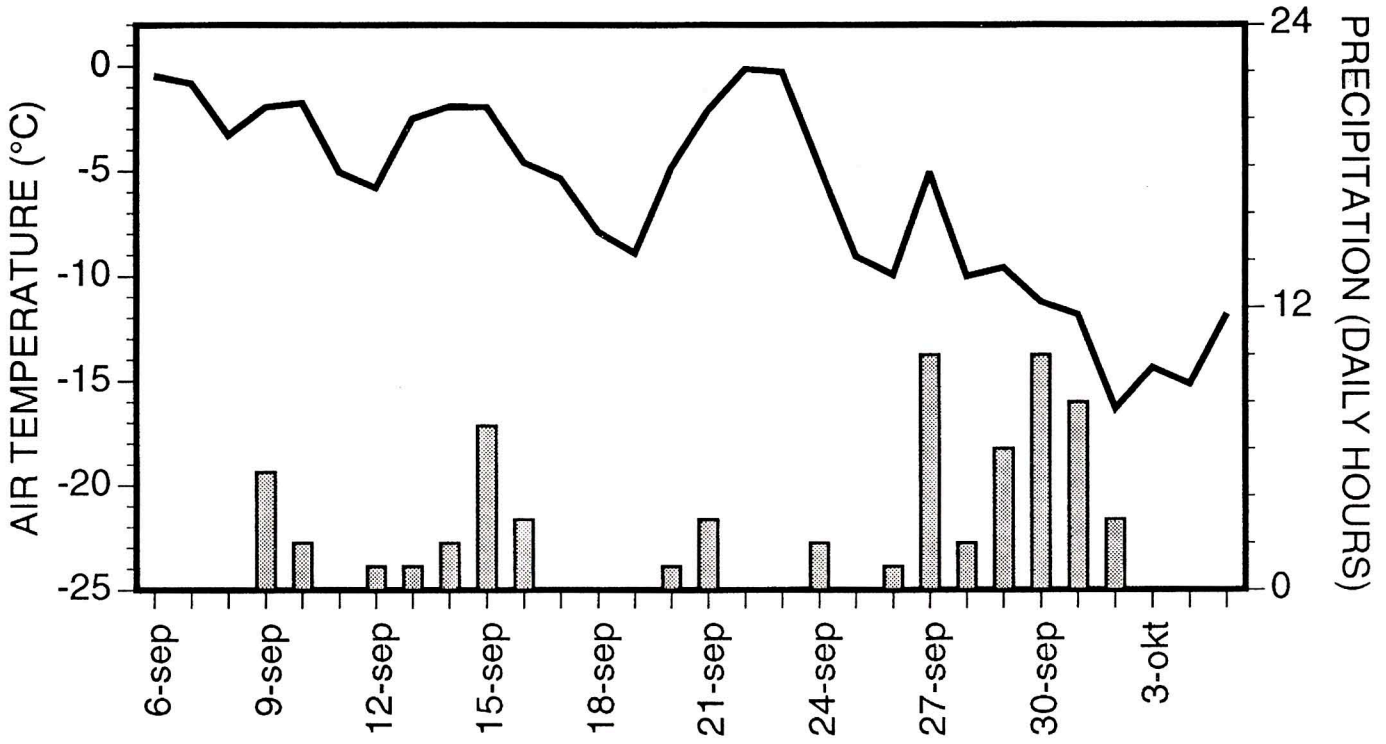

Fig. 2 - Daily average temperature and snow fall as recorded on the Oden bridge

5. EVOLUTION OF BACKSCATTER SIGNATURES

The ERS-1 SAR provides a unique opportunity to study time series of backscatter signatures. Fig. 3 shows the evolution of multi-year ice signatures from field stations RS 18 and 19 (stations and sites are numbered sequentially with RS as a prefix, e.g. RS 18:1 denotes site 1 at station 18) over a 12-day period. We note that the signature is remarkably stable which demonstrates the high precision of the radiometric calibration and the low temporal variability of the multi-year ice backscatter during the period.

Nilas and young ice do not show a stable signature due to the varying environmental conditions they may experience during growth. Fig. 4 shows two ERS-1 SAR images over the same area but separated by 3 days. The image from 26 September shows a high contrast between multi-year ice and the thin ice forms. There is essentially no open water in this image, and the different grey tones of the thin ice forms therefore correspond to different surface conditions. The appearance of the image from 29 September is quite different with little or no contrast between the multi-year and thin ice. This drastic change is due to a very rough and wet saline snow cover which developed from frost flowers and snow fall. Frost flowers were observed on the frozen lead (A in Fig. 4) on the evening of 26 September, and snow started to fall the day after. The falling snow destroyed the delicate frost flowers thereby forming a very rough and saline surface. This type of surface was observed on 29 September on young ice in an area outside Fig. 4.

Fig. 5 quantifies the principle signature variations of the thin ice forms. RS 18:1 and 19:2 represent young ice covered by old consolidated frost flowers, whereas A represents nilas with newly formed frost flowers. The latter formed on 26 September and probably turned into a rough and wet saline snow cover after the snow fall on 27 September. No field observations exist for the other areas but B and C are believed to represent similar young ice and nilas, respectively. We note that the nilas (A and C) shows a drastic increase in backscatter due to the snow fall, whereas the young ice (B) is more stable. The latter is probably due to the lower salinity which reduces the salt transport into the snow.

6. MODEL VS. BACKSCATTER MEASUREMENTS

Field measurements were made on eight different sites of thin ice forms. The surface roughness was sampled using a laser profiler which enabled the roughness spectrum to be accurately determined. Typically, 8-10 one-metre surface profiles were acquired at each measurement site in order to reduce statistical fluctuations. It was found that a combined exponential and Gaussian correlation function

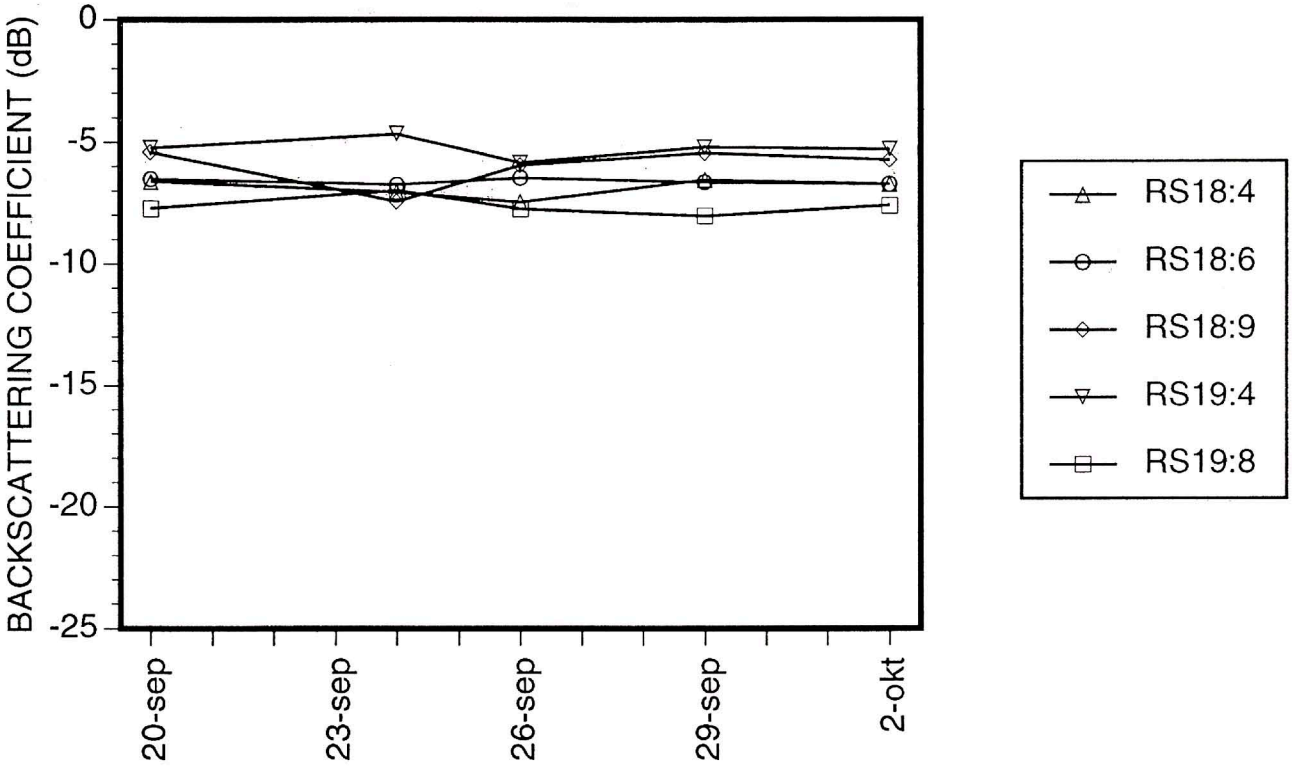

Fig. 3 - Backscatter signature evolution of level multi-year ice. The backscatter coefficient has been normalised to an incidence angle of 23° by assuming 0.1 dB/degree

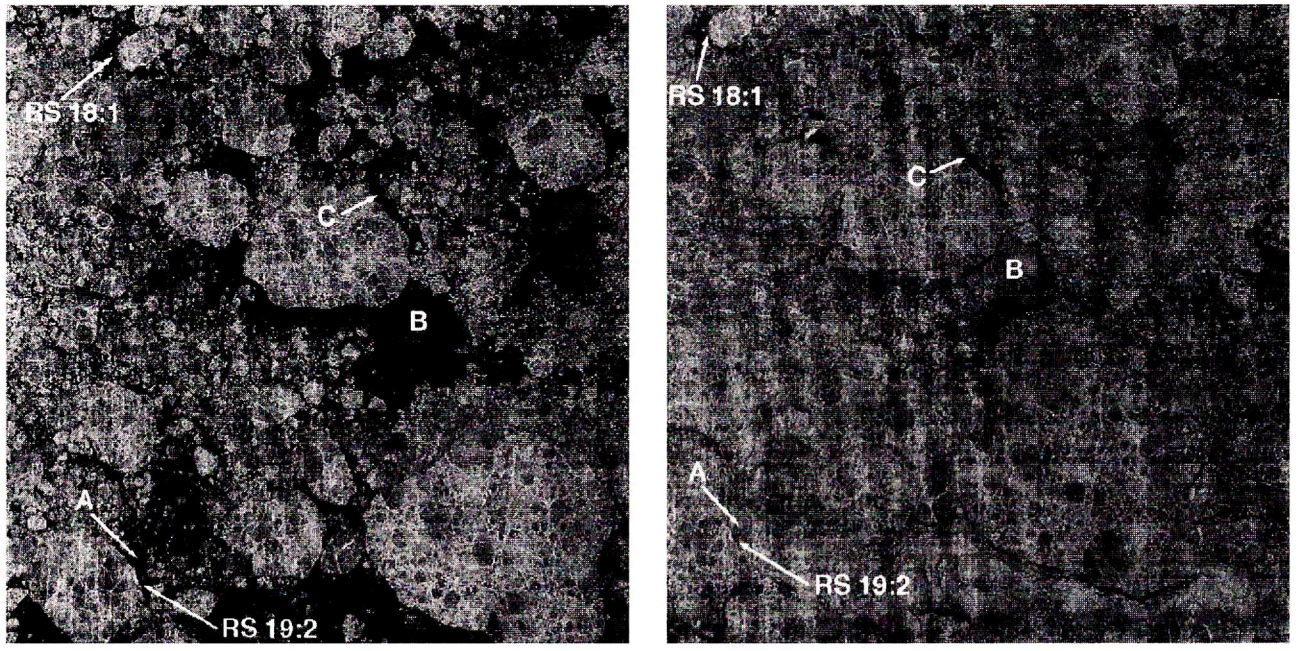

Fig. 4 - ERS-1 SAR images (63 x 63 km) acquired on (a) 26 September and (b) 29 September. Note the drastic increase of backscatter in the frozen leads. The location of the images is indicated in Fig. 1

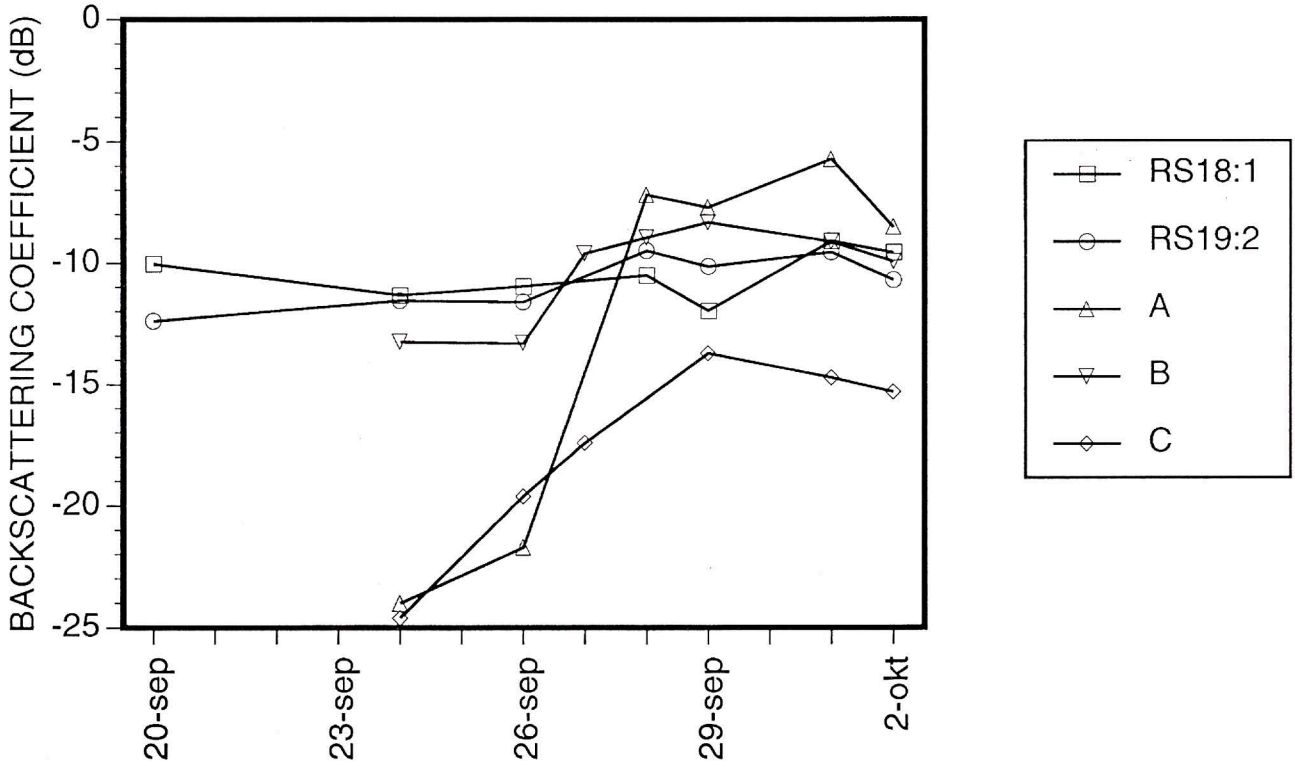

Fig. 5 - Evolution of nilas and young ice. The backscattering coefficient has been normalised to an incidence angle of 23° by assuming 0.3 dB/degree

(Fung *et al.* 1992) agrees well with the measured spectra, and each surface may be characterised by a rms height and two correlation length parameters. The temperature, salinity and density of the ice was measured in 10-cm samples which results in bulk quantities. Tables 1-3 summarise the measured and estimated parameters together with backscatter model calculations. When a parameter has been estimated, we indicate this by showing it in parenthesis. The tables also include estimates of the input parameter error and the root-sum-squared total error of the model.

Fig. 6 shows the results graphically with measured versus modelled backscattering coefficients. The agreement is good except for two cases when a significant discrepancy is found: RS 21:1 and RS 19:2. The difference is 6 dB for RS 21:1 which we believe indicates that the dominating backscatter originates from the interface between the thin snow cover and slush. Unfortunately, the snow made it impossible to measure the slush surface without destroying it, and the rms height given in Table 3 corresponds to the ice surface below the slush. The difference is 3 dB for RS 19:2 which we believe is associated with the dielectric constant. A probable explanation is that the surface salinity was lower than the measured bulk value since the periods with high air temperature drained brine from the surface.

Table 1 - Ice covered with frost flowers

Site	**RS 18:1**	**RS 19:2**	**RS 22:5**
Date	24/9/91	26/9/91	4/10/91
Air temperature (°C)	-5	-9	-16
Ice thickness (m)	0.14	0.16	0.08
Model input parameters:			
Surface temp. (°C)	-3 ± 0.5	(-5 ± 1)	(-7 ± 1)
Density (g/cm³)	0.86 ± 0.04	0.90 ± 0.05	(0.30 ± 0.06)
Salinity (ppt)	9.7 ± 1	14 ± 1	50 ± 5
Rms height (mm)	6.2	6.4	8.2
Gauss. correlation length (mm)	2.9	2.7	3.1
Exp. correlation length (mm)	8.4	17	8.3
Number of profiles	16	10	6
Incidence angle (°)	20.6	22.7	20.7
Model results:			
Brine volume (%)	15	14	12
Dielectric constant	4.1 - j 0.48	4.0 - j 0.44	3.7 -j 2.1
σ° model (dB)	-10.9 ± 0.4	-8.5 ± 0.4	$-12.1^{+1.1}_{-1.5}$
Measurement results:			
σ° measured (dB)	-10.8	-11.8	-13.6

Table 2 - Ice covered with saline snow

Site	RS 20:6	RS 22:2
Date	29/9/91	4/10/91
Air temperature (°C)	-9	-16
Ice thickness (m)	0.14	0.16
Model input parameters:		
Surface temp. (°C)	(-5 ± 1)	(-9 ± 1)
Density (g/cm^3)	(0.5 ± 0.1)	(0.5 ± 0.1)
Salinity (ppt)	40 ± 4	43 ± 4
Rms height (mm)	5.8	4.4
Gauss. correlation length (mm)	8.8	5.3
Exp. correlation length (mm)	12	12
Number of profiles	8	5
Incidence angle (°)	22.0	20.8
Model results:		
Brine volume (%)	22	14
Dielectric constant	5.8 -j 2.5	3.8 -j 1.0
σ° model (dB)	$-6.7^{+1.6}_{-2.5}$	$-10.4^{+1.4}_{-2.1}$
Measurement results:		
σ° measured (dB)	-6.0	-9.9

Table 3 - Ice covered with slush

Site	RS 20:1	RS 20:7	RS 21:1
Date	29/9/91	29/9/91	1/10/91
Air temperature (°C)	-9	-9	-11
Ice thickness (m)	0.17	0.10	0.12
Model input parameters:			
Surface temp. (°C)	(-5 ± 1)	(-4 ± 1)	-5 ± 0.5
Brine volume (%)	(40 ± 8)	(40 ± 8)	(40 ± 8)
Rms height (mm)	2.2	2.7	0.8
Gauss. correlation length (mm)	6.4	3.8	6.5
Exp. correlation length (mm)	10	4.7	2.1
Number of profiles	8	4	8
Incidence angle (°)	22.0	22.0	24.8
Model results:			
Dielectric constant	13 -j 6.3	14 -j 6.1	13 -j 6.3
σ° model (dB)	$-9.7^{+0.9}_{-1.1}$	$-12.2^{+1.0}_{-1.4}$	$-21.4^{+1.0}_{-1.2}$
Measurement results:			
σ° measured (dB)	-10.7	-14.2	-15.6

The results indicate that the backscatter signatures of thinner ice forms are very complicated, and that both the dielectric constant and the surface roughness are highly variable. This suggests that there is little correlation between backscattering coefficient and ice thickness as shown in Fig. 7, although it appears that the thinner ice (< 13 cm) has a lower backscattering coefficient than the thicker ice (> 13 cm).

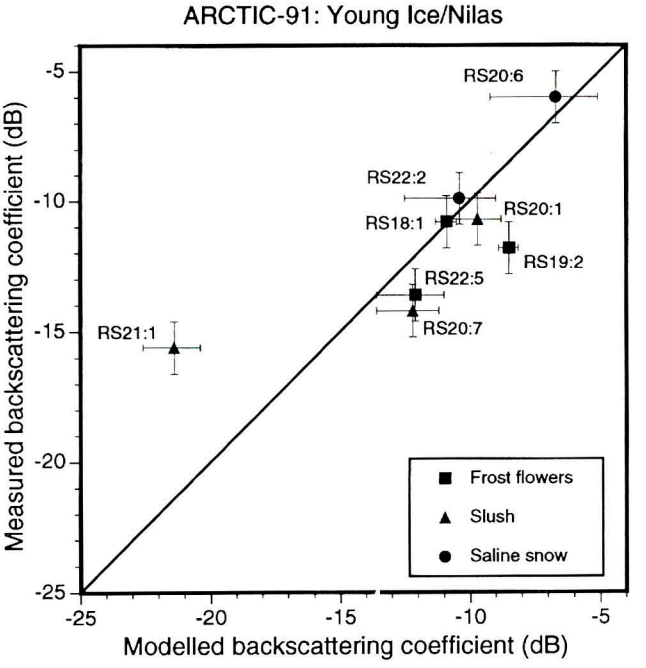

Fig. 6 - Measured backscattering coefficient vs. theoretical model

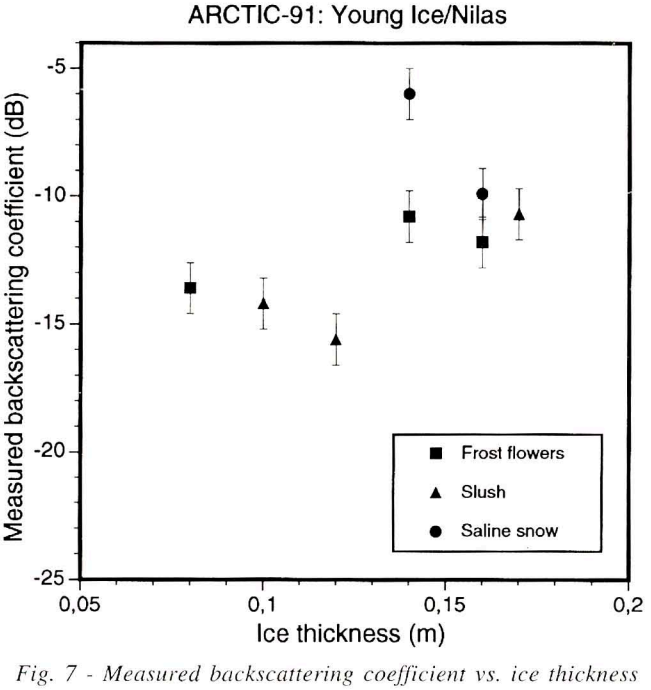

Fig. 7 - Measured backscattering coefficient vs. ice thickness

7. CONCLUSIONS

The evolution of thin ice forms in ERS-1 SAR images have been investigated based on *in situ* data from the ARCTIC-91 expedition. Air temperature dropped from 0°C to -16°C during the studied period and considerable ice growth was experienced. The backscatter signature evo-

lution was found to depend critically on the temperature and precipitation history of the ice. Ice with old frost flowers were relatively stable, whereas ice with newly formed frost flowers showed a large variability. The results indicate that parameter retrieval for thin ice forms will have to take temperature and precipitation variations into account.

The backscatter measurements were also compared with theoretical model calculations based on field measurements of ice and snow parameters. Most ice types show a 1-2 dB difference, but two cases of significant discrepancies were observed. More accurate models for surface scattering and dielectric properties would improve the possibilities to calculate the backscattering coefficient, especially for the frost flowers.

REFERENCES

Carlström A. & Ulander L.M.H., 1993, C-band Radar Backscatter Signatures of Old Sea Ice in the Central Arctic during Freeze Up, IEEE Trans. Geosci. Remote Sensing, 31, 819-829.

Cox G.F.N. & Weeks W.F., 1983, Equations for Determining the Gas and Brine Volumes in Sea-Ice Samples, J. Glaciol., 29, 306-316.

Drinkwater M.R. & Crocker G.B., 1988, Modelling Changes in the Dielectric and Scattering Properties of Young Snow-Covered Sea Ice at GHz Frequencies, J. Glaciol., 34, 274-282.

Fung A.K., Li Z. & Chen K.S., 1992, Backscattering from a Randomly Rough Dielectric Surface, IEEE Trans. Geosci. Remote Sensing, 30, 356-369.

Hallikainen M.T., Ulaby F.T. & Abdelrazik M., 1986, Dielectric Properties of Snow in the 3 to 37 GHz Range, IEEE Trans. Antennas Propagat., 34, 1329-1341.

Kim Y.-S., Onstott R.G. & Moore R.K., 1984, The Effect of a Snow Cover on Microwave Backscatter from Sea Ice, IEEE J. Oceanic Eng., 9, 383-388.

Kim Y.-S., Moore R.K., 1985, Onstott R.G. & Gogineni S., Towards Identification of Optimum Radar Parameters for Sea-Ice Monitoring, J. Glaciol., 31, 214-219.

Laur H., 1992, ERS-1 SAR Calibration, Derivation of Backscatter Coefficient σ° in ERS-1.SAR.PRI products, Issue 1, Rev 0, ESA-ESRIN.

Livingstone C.E. & Drinkwater M.R., 1991, Springtime C-band SAR Backscatter Signatures of Labrador Sea Marginal Ice: Measurements vs. Modelling Predictions, IEEE Trans. Geosci. Remote Sensing, 29, 29-41. (Correction, IEEE Trans. Geosci. Remote Sensing, 29, 472, 1991.)

Maykut G.A., 1978, Energy Exchange over Young Sea Ice in the Central Arctic, J. Geophys. Res., 83, 3646-3658.

Maykut G.A., 1982, Large-Scale Heat Exchange and Ice Production in the Central Arctic, J. Geophys. Res., 87, 7971-7984.

Stogryn A. & Desargant A., 1985, The Dielectric Properties of Brine in Sea Ice at Microwave Frequencies, IEEE Trans. Antennas Propagat., 33, 523-532.

Thorndike A.S., Rothrock D.A., Maykut G.A. & Colony R., 1975, The Thickness Distribution of Sea Ice, J. Geophys. Res., 80, 4501-4513.

Ulander L.M.H., 1991, Accuracy of Using Point Targets for SAR Calibration, IEEE Trans. Aerospace Electron Syst., 27, 139-148.

Ulander L.M.H., 1992, Calibration of the ERS-1 SAR Fast-Delivery Images, Proceedings of the First ERS-1 Symposium, Space at the Service of our Environment, held in Cannes, 4-6 Nov 1992, ESA SP-359, 173-178.

Ulander L.M.H., Johansson R. & Askne J., 1992, C-band Radar Backscatter of Baltic Sea Ice: Theoretical Predictions Compared with Calibrated SAR Measurements, Int. J. Remote Sensing, 13, 2447-2468.

Vant M.R., Ramseier R.O. & Makios V., 1978, The Complex-Dielectric Constant of Sea Ice at Frequencies in the Range 0.1-40 GHz, J. Appl. Phys., 49, 1264-1280.

Winebrenner D.P., Bredow J., Fung A.K., Drinkwater M.D., Nghiem S., Gow A.J., Perovich D.K., Grenfell T.C., Han H.C., Kong J.A., Lee J.K., Mudaliar R., Onstott R.G., Tsang L. & West R.D., 1992, Microwave Sea Ice Signature Modeling, In: Microwave Remote Sensing of Sea Ice, Geophysical Monograph 68, Americal Geophysical Union, 137-175.